processes

MDPI

*Article*

# Process Evaluation of Staged Self-Diverting Acidizing and Cationic Polymer Sand Stabilization in Unconsolidated Sandstone

**Yixin Pan [1], Shijun Chen [1,*], Siqi Zheng [1], Li Liao [2], Qi Jiang [2] and Dan Gao [3]**

[1] College of Chemistry and Chemical Engineering, Xi'an Petroleum University, Xi'an 710065, China; 24212071168@stumail.xsyu.edu.cn (Y.P.); 24212071181@stumail.xsyu.edu.cn (S.Z.)
[2] Oil and Gas Technology Institute, PetroChina Qinghai Oilfield Company, Dunhuang 736200, China; liaoliqh@petrochina.com.cn (L.L.); jiangqiqh@petrochina.com.cn (Q.J.)
[3] The Sixth Oil Production Plant of Changqing Oilfield Branch, Xi'an 710000, China; gaodan_cq@petrochina.com.cn
* Correspondence: csjun@xsyu.edu.cn

**Abstract**

Unconsolidated sandstone gas reservoirs often suffer from near-wellbore plugging, permeability contrast, and sand production after acid stimulation. This study evaluates a staged chemical process that couples limited cationic polymer sand stabilization with reaction-induced self-diverting acidizing, instead of direct premixing or simultaneous co-injection of acid and sand control fluids. Residual acid viscosity tests, core flooding experiments, dynamic sand production tests, scanning electron microscopy/energy-dispersive spectroscopy, and low-field nuclear magnetic resonance measurements were used to investigate viscosity building, diversion, permeability retention, and pore structure evolution. The 5 wt% EAB self-diverting acid exhibited the strongest reaction-induced viscosity-building behavior, reaching a residual acid viscosity of 134 mPa·s. The selected HCl + HF acid system produced a clear temporary-plugging response during core flooding, and the optimized 0.2 wt% cationic polyacrylamide stabilizer increased the critical sand production flow rate to 1.8 mL·min$^{-1}$ while maintaining acceptable permeability recovery. Microscopic evidence indicates improved pore connectivity without large-scale skeletal collapse. A comprehensive synergy index showed that medium-permeability cores (300–500 mD) achieved the best balance among acid diversion, sand stabilization, and permeability retention. The proposed process provides a laboratory-scale foundation for coupled stimulation and sand control design.

**Keywords:** reaction-induced viscosity building; self-diverting acidizing; cationic polyacrylamide; sand stabilization; core flooding; porous media transport; unconsolidated sandstone; permeability retention

Check for updates

Received: 14 July 2026
Revised: 16 August 2026
Accepted: 25 August 2026
Published: 28 August 2026

**Copyright:** © 2026 by the authors. Licensee MDPI, Basel, Switzerland. This article is an open access article distributed under the terms and conditions of the Creative Commons Attribution (CC BY) license.

## 1. Introduction

Low-pressure unconsolidated sandstone gas reservoirs are commonly affected by weak cementation, permeability contrast, near-wellbore plugging, and sand production after stimulation [1–3]. Matrix acidizing can remove formation damage and improve pore connectivity, but preferential acid entry into high-permeability channels and excessive cement dissolution may aggravate fines migration and framework instability [4].

Chemical sand stabilization reduces particle detachment through polymer adsorption, bridging, or weak cementation [5]. However, strong consolidation or excessive polymer retention may block pore throats and impair injectivity. VES-based self-diverting acids can

generate residual acid viscosity after acid–rock reaction and redirect acid from dominant channels to less contacted zones [6–10], but previous studies have mainly considered acid diversion and sand stabilization separately [11]. Coupled particle transport and structural stability issues reported in geothermal, $CO_2$-fracturing, and hydrate reservoir studies also indicate the need to evaluate stimulation and stability together [12–15].

The knowledge gap is the lack of a process-oriented evaluation of staged sand stabilization, followed by self-diverting acidizing in unconsolidated sandstone. This work distinguishes staged placement from direct premixing, links residual acid viscosity, pressure response, dynamic sand production, SEM–EDS, and LF-NMR evidence, and identifies the permeability range in which diversion, sand control, and permeability retention can be balanced. The results provide practical guidance for designing combined acidizing and sand control treatments in low-pressure unconsolidated sandstone reservoirs.

## 2. Materials and Methods

### 2.1. Materials and Instruments

The acid systems included HCl, HF, $HBF_4$, and viscoelastic-surfactant-based self-diverting acid agents, including EAB, OAB, and dodecyl hydroxypropyl phosphate betaine. Candidate sand stabilization systems included cationic polyacrylamide polymer A (80-mesh), cationic polyacrylamide polymer B (40-mesh), low-molecular-weight polyacrylamide (PAM), hexamethyldisiloxane (HMDSO), aminopropyl diethoxy methylsilane (APDEMS), formation water, and reservoir core and sand samples. Calcium carbonate was used to simulate the increase in $Ca^{2+}$ concentration after the acid–rock reaction. In this paper, the term "integrated treatment" refers to staged interaction between the sand stabilizer slug and the self-diverting acid slug, rather than long-duration premixing of strong acid and sand stabilizer solutions. In the slug ratio experiments, the volume ratio between the sand stabilizer and the main acid refers to the slug–volume ratio (see Table 1).

**Table 1.** Main chemical materials and their structural features.

| Material Category | Representative Materials | Main Structural Features |
| --- | --- | --- |
| Self-diverting acid agents | EAB, OAB, dodecyl hydroxypropyl phosphate betaine | Long-chain hydrophobic groups and amphoteric/ionic hydrophilic head groups; divalent ions and salinity after acid–rock reaction promote entangled micelles. |
| Inorganic acid system | HCl, HF, $HBF_4$ | $H^+$ provides dissolution capacity; HF/$HBF_4$ reacts with aluminosilicates, clays, and some cementing materials. |
| Polymeric sand stabilizers | Cationic polyacrylamide A/B, PAM | Polyacrylamide backbone with cationic modification; enhances adsorption on negatively charged sand/clay surfaces. |
| Organosilicon sand stabilizers | HMDSO, APDEMS | Si–O–Si or Si–OR structures; amino silane can hydrolyze and condense into a siloxane network. |

The main instruments included a ZNN-D12 digital rotational viscometer, a DQ-IV plugging/profile control evaluation apparatus, an SEM–EDS apparatus, and an LF-NMR analyzer.

The acid systems included hydrochloric acid (HCl), hydrofluoric acid (HF), tetrafluoroboric acid ($HBF_4$), and viscoelastic-surfactant-based self-diverting acid agents. HCl, HF, and $HBF_4$ were purchased from Tianjin Damao Chemical Reagent Partnership Enterprise (Tianjin, China). Erucamidopropyl betaine (EAB), oleamidopropyl betaine (OAB), dodecyl hydroxypropyl phosphate betaine, cationic polyacrylamide polymer A, cationic polyacry-

lamide polymer B, low-molecular-weight polyacrylamide (PAM), hexamethyldisiloxane (HMDSO), aminopropyl diethoxy methylsilane (APDEMS), calcium carbonate, and calcium chloride were purchased from Shanghai Macklin Biochemical Technology Co., Ltd. (Shanghai, China). Formation water, reservoir cores, and sand samples were provided by PetroChina Qinghai Oilfield Company (Dunhuang, China). The main instruments included a ZNN-D12 digital rotational viscometer (Nanbei Instrument Limited, Zhengzhou, China), a DQ-IV plugging/profile-control evaluation apparatus (Jiangsu Huaan Scientific Instrument Co., Ltd., Haian, China), SEM–EDS equipment tested by Xi'an Yancheng Technology Co., Ltd. (Xi'an, China), and a low-field nuclear magnetic resonance analyzer (Suzhou Niumag Analytical Instrument Co., Ltd., Suzhou, China).

### 2.2. Evaluation of Reaction-Induced Self-Diverting Acid Behavior

The diversion potential of different viscoelastic surfactant systems was compared by measuring the residual acid viscosity after reaction with calcium carbonate. Apparent viscosity was measured for different surfactant types, concentrations, and $Ca^{2+}$ concentrations. Single-core flooding experiments were used to characterize temporary plugging and diversion. Cores with different permeabilities were loaded into the flooding apparatus. Formation water was first injected to establish a stable baseline pressure. The self-diverting acid was then pumped at a constant rate, and the injection pressure was recorded as a function of injected pore volume (PV). Formation water was subsequently injected to evaluate pressure recovery and post-treatment permeability. Core permeability was calculated using Darcy's law:

$$K = Q\mu L/(A\Delta P) \quad (1)$$

where $K$ is permeability, $Q$ is flow rate, $\mu$ is fluid viscosity, $L$ is core length, $A$ is cross-sectional area, and $\Delta P$ is the pressure drop.

During the 300 mD self-diverting acid flooding experiment, effluent samples were collected at selected PV values during acid injection and subsequent flushing. Apparent viscosity, pH, and visual state were recorded. The same samples were filtered through a 0.45 μm membrane, and the suspended solids content was measured after blank correction. These tests were used to link the pressure response with residual acid viscosity and fines migration. To clarify the relationship between viscosity and temperature for the 5 wt% EAB system, temperature-dependent tests were conducted at 25–80 °C, and apparent viscosity, pH, conductivity, and visual state were recorded.

### 2.3. Evaluation of Cationic Polymer Sand Stabilization

A sand stabilizer screening study was first conducted to address the sand production tendency of low-pressure unconsolidated sandstone after acidizing [16]. Candidate polymeric and organosilicon systems were compared based on their material structure, solution viscosity, critical sand production flow rate, and dynamic sand stabilization performance. In the critical sand production test, reservoir sand samples from the same batch were packed into sand-filled models. After injection and aging of the stabilizer solution, the displacement rate was increased stepwise, and sand production at the outlet was monitored.

Dynamic sand stabilization experiments were conducted to evaluate the performance of the stabilizer under flow-induced erosion. Reservoir sand was packed into a sand tube. Formation water was injected to determine initial permeability. A designed volume of stabilizer solution was then injected and aged, followed by reinjection of formation water. Sand production, the maximum pressure difference, and permeability recovery were recorded as the primary evaluation indicators [17]. This method evaluates both sand control capacity and its additional influence on flow channels, thereby preventing overinterpretation based only on the absence of sand production (see Figure 1).

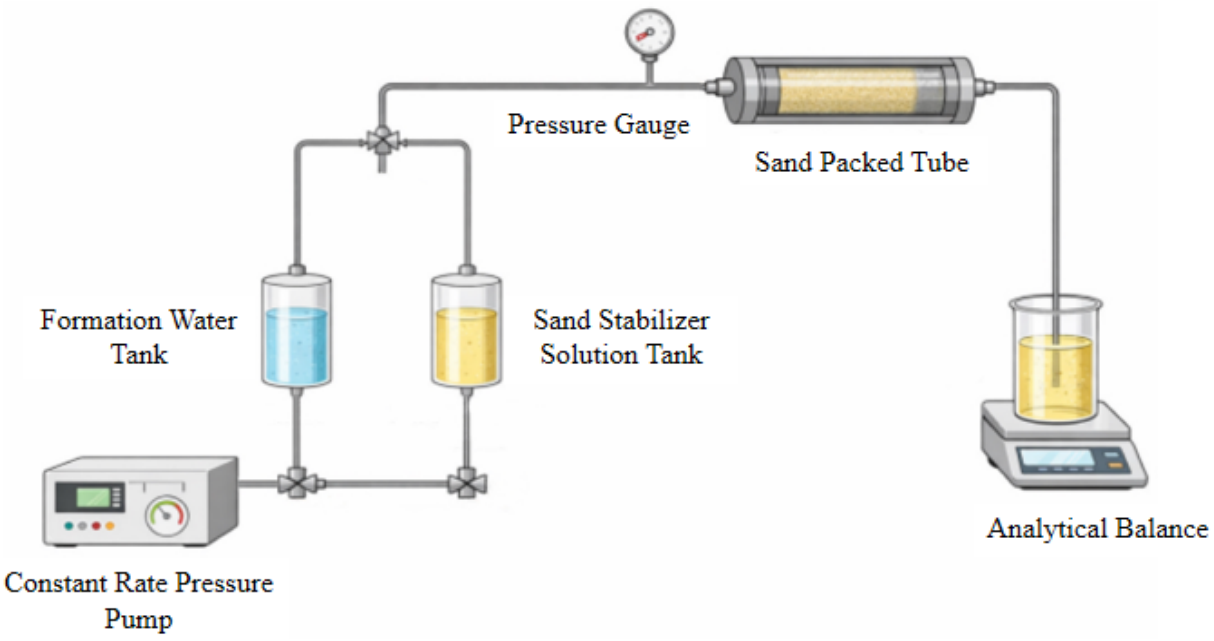



**Figure 1.** Schematic workflow of the dynamic sand stabilization evaluation experiment.

### *2.4. Staged Coupling Process and Microscopic Characterization*

After screening the acid and sand stabilizer systems, a staged integrated process was designed and evaluated. Four groups were compared: acidizing alone, sand stabilization alone, sand stabilization followed by acidizing, and a premixing boundary control group. The sand-stabilization-followed-by-acidizing group represents the recommended process: 0.2 wt% cationic polyacrylamide (80-mesh) was first injected to form a limited near-wellbore sand stabilization layer. After aging, the self-diverting acid was injected to achieve reaction-induced viscosity building and deep diversion. The premixing boundary control group was included only to assess possible pressure response and compatibility risks when acid contacts the stabilizer and does not represent a recommended field procedure. Different slug ratios between the sand stabilizer and the main acid were evaluated to define the process window.

For the premixing boundary control test, the 0.2 wt% cationic polymer stabilizer and optimized self-diverting acid were mixed at a 1:1 volume ratio. Viscosity was measured after 0–240 min of contact, and a 300 mD core flooding test was conducted after 30 min of premixing to record the pressure–PV response.

To evaluate permeability applicability, staged integrated core flooding experiments were conducted using cores with permeabilities of approximately 1–1000 mD, including intermediate-permeability cores. In addition, reservoir temperature verification was performed at 50 °C using 300 and 500 mD cores. All experiments followed the same sequence: formation water baseline flooding, 0.2 wt% stabilizer injection, aging, self-diverting acid injection, and subsequent formation water flushing. The pressure response, critical sand production flow rate, permeability retention, and SI were calculated, and weight sensitivity was examined to verify the stability of the ranking.

SEM was used to observe the surface morphology of sand grains and rock samples before and after treatment. The SEM–EDS samples included medium-permeability sandstone cores before and after self-diverting acid flooding, where the acid-treated specimens were collected from the inlet side of an approximately 300 mD core; original reservoir sand and sand treated with 0.2 wt% 80-mesh cationic polyacrylamide; and parallel sandstone cores before and after staged treatment. EDS was used to assess acid-derived elemental distributions, soluble component changes, and ion enrichment. LF-NMR measurements

were conducted on parallel medium-permeability unconsolidated sandstone cores before and after staged treatment [18]. Samples were saturated with formation water before testing to ensure comparable T2 spectra and calculated porosity.

## 3. Results and Discussion

### *3.1. Reaction-Induced Viscosity Building and Acid Diversion*

#### 3.1.1. Screening of Self-Diverting Acid Agents

Table 2 shows the apparent viscosity of various self-diverting acid agents after reaction with calcium carbonate. The 5 wt% EAB system exhibited the strongest diversion response, achieving a maximum room-temperature viscosity of 134 mPa·s at 8 wt% calcium carbonate. EAB contained both hydrophobic chains and ionic/amphoteric head groups. During the fresh-acid stage, the system maintained relatively low viscosity, thereby preserving injectivity. After the acid–rock reaction, increased $Ca^{2+}$ and $Mg^{2+}$ concentrations promoted micellar transformation from a weakly entangled state to wormlike or network structures, producing substantial residual acid viscosity building. Accordingly, the primary advantage of the viscoelastic surfactant (VES)-based system is its ability to generate viscosity after the acid–rock reaction rather than through a high initial fresh-acid viscosity [19] (see Figure 2).

**Table 2.** Screening of self-diverting acid agents at different calcium carbonate concentrations.

| Conc. | Agent | 4% | 6% | 8% | 10% | 12% | 14% | 16% | 18% |
|---|---|---|---|---|---|---|---|---|---|
| 5% | EAB | 74 | 89 | 134 | 47 | 0 | 0 | 0 | 0 |
| 5% | OAB | 0 | 0 | 45 | 104 | 74 | 0 | 0 | 0 |
| 5% | Solid self-diverting acid | 0 | 0 | 51 | 45 | 9 | 0 | 0 | 0 |
| 5% | Dodecyl hydroxypropyl phosphate betaine | 0 | 0 | 0 | 0 | 0 | 3 | 3 | 0 |
| 3% | EAB | 0 | 45 | 74 | 60 | 30 | 0 | 0 | 0 |
| 3% | OAB | 0 | 0 | 0 | 0 | 36 | 6 | 0 | 0 |
| 3% | Solid self-diverting acid | 0 | 0 | 21 | 21 | 6 | 0 | 0 | 0 |

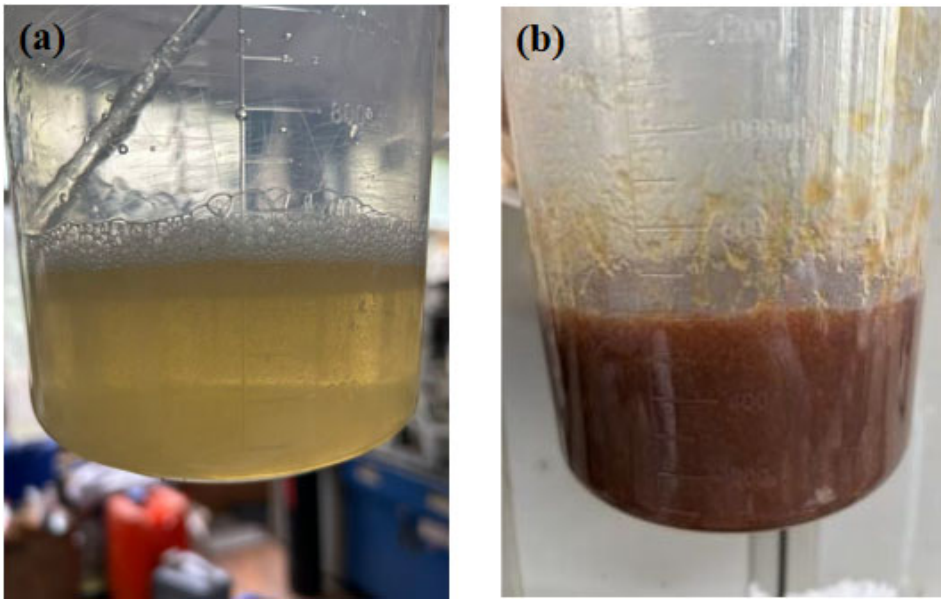



**Figure 2.** Visual comparison of (**a**) fresh acid without corrosion inhibitor and (**b**) the solution after acid–rock reaction.

Temperature-dependent residual acid tests were performed to verify whether the 5 wt% EAB system remained effective under reservoir temperature conditions (Table 3).

**Table 3.** Effects of temperature on the residual acid viscosity of the 5 wt% EAB system at 8 wt% $CaCO_3$.

| Temperature/°C | $CaCO_3$/wt% | Apparent Viscosity/mPa·s | Viscosity Retention/% | pH |
|---|---|---|---|---|
| 25 | 8 | 134.0 | 100.0 | 1.38 |
| 40 | 8 | 126.3 | 94.3 | 1.42 |
| 50 | 8 | 118.7 | 88.6 | 1.46 |
| 60 | 8 | 104.5 | 78.0 | 1.51 |
| 80 | 8 | 69.2 | 51.6 | 1.60 |

At 8 wt% $CaCO_3$, the viscosity decreased from 134.0 mPa·s at 25 °C to 118.7 mPa·s at 50 °C, indicating that the system still retained a strong viscosity-building capacity at a representative reservoir temperature. Further heating reduced viscosity to 104.5 mPa·s at 60 °C and 69.2 mPa·s at 80 °C, suggesting that elevated temperature weakened micellar entanglement. Therefore, the EAB system was suitable for the 50 °C core flooding verification, but its diversion capacity may decline at higher temperatures.

### 3.1.2. Temporary Plugging and Diversion During Core Flooding

Core flooding experiments using different acid systems were conducted to identify the preferred acid composition. As shown in Figure 3, the HF-containing system generated greater flow resistance and a stronger flooding response than the $HBF_4$ system. HF reacted more effectively with reactive aluminosilicates, clay minerals, and cementing components in sandstone. This reaction promoted divalent-ion release, enhanced residual-acid viscosity, and formed dissolution channels. However, greater dissolution also increased the risk of fines detachment and particle migration in the absence of skeletal stabilization. Accordingly, subsequent experiments adopted staged coupling of acidizing and chemical sand stabilization rather than simply increasing acid strength.

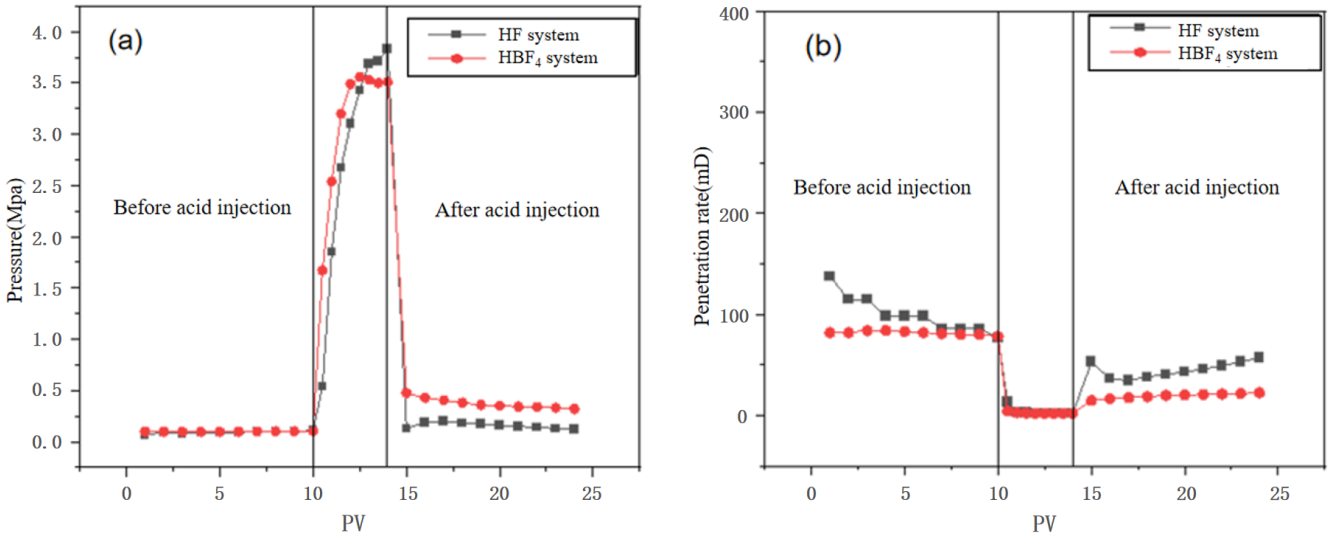



**Figure 3.** Core flooding response for different acid systems: (**a**) injection pressure versus injected PV and (**b**) permeability versus injected PV.

The HF system was further evaluated using cores with different permeabilities (Figure 4). During acid injection, the injection pressure increased, whereas apparent permeability generally decreased, demonstrating temporary plugging and diversion. After continued formation-water injection and a 24 h shut-in period, permeability recovered relative to that during the acid-injection stage, confirming partial cleanup and flowback

capability. Medium- and low-permeability cores exhibited a stronger temporary-plugging and diversion response, whereas the high-permeability sample was more strongly affected by dominant channels.

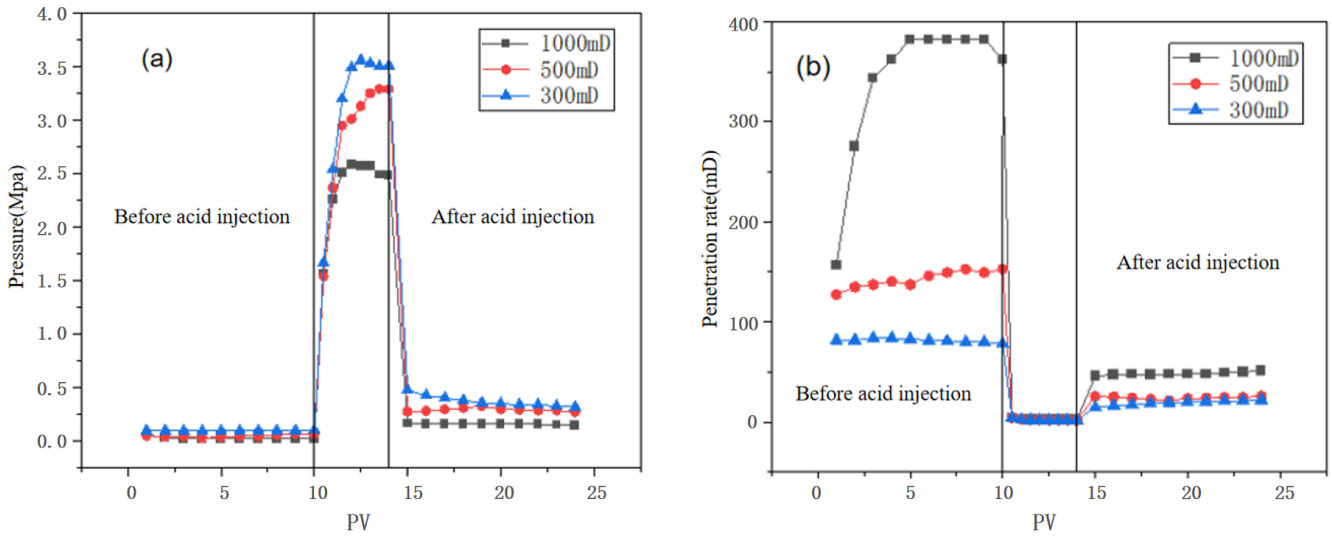



**Figure 4.** Core flooding behavior of cores with different permeabilities: (**a**) injection pressure versus injected PV and (**b**) permeability versus injected PV.

Effluent viscosity was measured during the 300 mD acid flooding test to support the pressure response interpretation (Table 4).

**Table 4.** Variation in effluent viscosity during self-diverting acid flooding.

| Stage | Acid/Post-Flush PV | Pressure/MPa | Effluent Viscosity/mPa·s | pH |
|---|---|---|---|---|
| Early acid inj. | 0.5 | 0.42 | 6.8 | 0.78 |
| Early acid inj. | 1.0 | 0.86 | 14.5 | 0.92 |
| Reaction growth | 1.5 | 1.58 | 31.6 | 1.18 |
| Reaction growth | 2.0 | 2.36 | 54.8 | 1.46 |
| Peak viscosity | 3.0 | 3.18 | 78.5 | 1.83 |
| Peak viscosity | 4.0 | 3.82 | 91.7 | 2.15 |
| Late acid inj. | 5.0 | 3.98 | 84.3 | 2.31 |
| Early flush | 1.0 | 0.82 | 34.6 | 2.72 |
| Middle flush | 3.0 | 0.56 | 11.8 | 3.05 |
| Late flush | 5.0 | 0.44 | 3.6 | 3.28 |

The effluent viscosity increased from 6.8–14.5 mPa·s at the early acid injection stage to 91.7 mPa·s at 4.0 PV, then decreased to 3.6 mPa·s during late post-flush. This confirms reaction-induced residual acid viscosity buildup and partial cleanup after water flooding.

The suspended solids concentration was also measured to evaluate fines migration during acid flooding (Table 5).

Suspended solids increased from 18.6–32.4 mg·L$^{-1}$ at the early stage to a peak of 176.2 mg·L$^{-1}$ at 3.0 PV, then decreased during later injection. Therefore, fines migration contributed to flow resistance variation, but the sustained pressure response was more consistent with the combined effects of residual acid viscosity, acid–rock reaction, and local pore throat changes.

**Table 5.** Variation in suspended solids concentration of effluent during self-diverting acid flooding.

| Stage | Injected Acid/Water PV | Pressure/MPa | Effluent Viscosity/mPa·s | Suspended Solids/mg·L$^{-1}$ |
|---|---|---|---|---|
| Early acid injection | 0.5 | 0.42 | 6.8 | 18.6 |
| Early acid injection | 1.0 | 0.86 | 14.5 | 32.4 |
| Enhanced acid–rock reaction | 1.5 | 1.58 | 31.6 | 74.8 |
| Enhanced acid–rock reaction | 2.0 | 2.36 | 54.8 | 128.5 |
| Peak fines release | 3.0 | 3.18 | 78.5 | 176.2 |
| Peak viscosity buildup | 4.0 | 3.82 | 91.7 | 149.6 |
| Late acid injection | 5.0 | 3.98 | 84.3 | 96.4 |
| Early post-flush | 1.0 | 0.82 | 34.6 | 68.5 |
| Middle post-flush | 3.0 | 0.56 | 11.8 | 29.7 |
| Late post-flush | 5.0 | 0.44 | 3.6 | 12.9 |

#### 3.1.3. SEM–EDS Evidence After Acid Flooding

A 300 mD sandstone core was selected for SEM–EDS analysis after flooding. Table 6 summarizes the elemental composition before and after acid treatment. Carbon and oxygen contents decreased after acidizing, indicating reactions between the acid and carbon- and oxygen-containing components. The appearance of F and Cl reflects the introduction of acid components. Increased Mg and Ca contents indicate ion enrichment after the acid–rock reaction, consistent with the observed residual acid viscosity building and temporary plugging behavior.

**Table 6.** EDS elemental composition of the core before and after acid flooding, reported as normalized atomic percentages (at.%).

| Element | Before Acidizing/at.% | After Acidizing/at.% |
|---|---|---|
| C | 36.70 | 18.09 |
| O | 32.15 | 24.82 |
| F | 0 | 3.87 |
| Mg | 1.96 | 3.52 |
| Al | 5.79 | 6.51 |
| Si | 9.61 | 21.55 |
| Cl | 0 | 21.64 |
| Ca | 13.80 | 18.09 |
| Total | 100 | 100.00 |

SEM micrographs (Figure 5) revealed increased surface roughness, irregular dissolution pits, and localized micropore development after acid treatment. Pore boundaries became more distinct and local pore space increased, suggesting improved pore connectivity. Simultaneously, broken particle edges, fines detachment, and localized loosening were observed. These features indicate that acidizing improved flow capacity but may have weakened the local granular framework. This observation explains why acidizing alone cannot simultaneously achieve damage removal and post-treatment sand control and underscores the need for limited near-wellbore sand stabilization before self-diverting acid treatment.

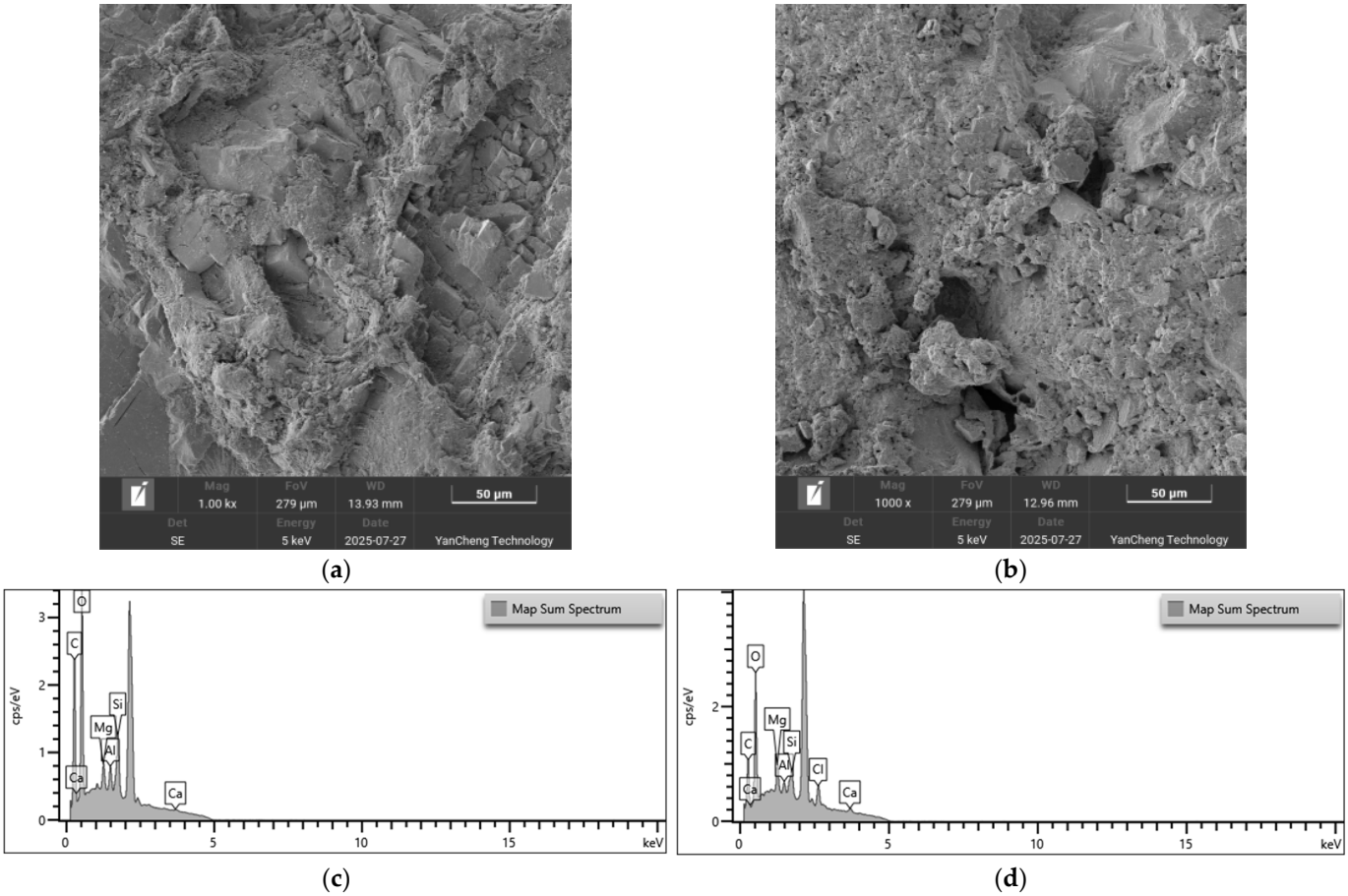



**Figure 5.** SEM micrographs and EDS spectra of the sandstone core before and after acid flooding: (**a**) SEM micrograph before acid flooding, (**b**) SEM micrograph after acid flooding, (**c**) EDS spectrum before acid flooding, and (**d**) EDS spectrum after acid flooding.

### *3.2. Sand Control and Permeability Retention Characteristics*

#### 3.2.1. Screening of Sand Stabilizer

Candidate stabilizers with different mechanisms were prepared at mass fractions of 0.1 wt% and 0.2 wt%. Table 7 lists their measured viscosities. Low-molecular-weight PAM, HMDSO, and APDEMS exhibited near-zero apparent viscosity under the test conditions and did not form effective stabilization structures. Cationic polyacrylamide polymers A and B exhibited higher viscosities because their amide and cationic functional groups promoted electrostatic adsorption and polymer chain bridging on quartz, clay minerals, and sand particle surfaces. These two polymers were selected for further evaluation and hereafter referred to as cationic polyacrylamide (80-mesh) and cationic polyacrylamide (40-mesh) (see Table 7).

**Table 7.** Viscosity of candidate sand stabilizer systems.

| Stabilizer | A 0.1% | A 0.2% | B 0.1% | B 0.2% | PAM 0.1% | PAM 0.2% | HMDSO 0.1% | HMDSO 0.2% | APDEMS 0.1% | APDEMS 0.2% |
|---|---|---|---|---|---|---|---|---|---|---|
| Viscosity, mPa·s | 21 | 36 | 15 | 21 | 0 | 0 | 0 | 0 | 0 | 0 |

#### 3.2.2. Critical Sand Production Flow Rate

Table 8 shows the critical sand production flow rates. No sand production occurred in any group below 1.0 mL·min$^{-1}$, showing that all polymeric stabilizer solutions provided some degree of stabilization. At 1.0 mL·min$^{-1}$, the 0.1 wt% 40-mesh cationic poly-

acrylamide group was the first to exhibit sand production. At 1.5 mL·min$^{-1}$, only the 0.2 wt% 80-mesh cationic polyacrylamide group remained sand-free. At 1.8 mL·min$^{-1}$, sand production occurred in all groups. Among the tested formulations, 0.2 wt% cationic polyacrylamide (80-mesh) exhibited the best sand stabilization performance.

**Table 8.** Critical sand production behavior of different sand stabilizer systems.

| Flow Rate, mL·min$^{-1}$ | 0.1% 80-Mesh CPAM | 0.2% 80-Mesh CPAM | 0.1% 40-Mesh CPAM | 0.2% 40-Mesh CPAM |
|---|---|---|---|---|
| 0.1 | No | No | No | No |
| 0.2 | No | No | No | No |
| 0.3 | No | No | No | No |
| 0.5 | No | No | No | No |
| 0.8 | No | No | No | No |
| 1.0 | No | No | Yes | No |
| 1.2 | Yes | No | Yes | No |
| 1.5 | Yes | No | Yes | Yes |
| 1.8 | Yes | Yes | Yes | Yes |

### 3.2.3. Dynamic Sand Stabilization Performance

Dynamic stabilization experiments were conducted using the 80-mesh cationic polyacrylamide system at different concentrations and flow rates. As shown in Table 9, the 0.2 wt% system exhibited lower sand production than the 0.1 wt% system at all flow rates. At 5 mL·min$^{-1}$, sand production decreased to $1.458 \times 10^{-5}$ g·mL$^{-1}$. However, improved sand control does not necessarily translate into superior overall performance. As polymer concentration increased, the maximum pressure differential increased and permeability decreased, indicating that particle bridging and limited cementation introduced additional flow resistance. Therefore, stabilizers for low-pressure gas reservoirs should provide effective sand control while minimizing plugging. The 0.2 wt% 80-mesh cationic polyacrylamide system achieved this balance, and the post-treatment permeability recovered to more than 70% of the initial sand pack permeability.

**Table 9.** Dynamic sand stabilization results for 80-mesh cationic polyacrylamide.

| Flow Rate, mL·min$^{-1}$ | Sand Production 0.1%, g·mL$^{-1}$ | Sand Production 0.2%, g·mL$^{-1}$ | Max ΔP 0.1%, MPa | Max ΔP 0.2%, MPa | Permeability 0.1%, mD | Permeability 0.2%, mD |
|---|---|---|---|---|---|---|
| 2 | $3.675 \times 10^{-4}$ | $1.075 \times 10^{-4}$ | 0.016 | 0.041 | 269 | 105 |
| 3 | $1.023 \times 10^{-4}$ | $8.372 \times 10^{-5}$ | 0.035 | 0.064 | 184 | 101 |
| 4 | $5.90 \times 10^{-5}$ | $4.883 \times 10^{-5}$ | 0.044 | 0.087 | 196 | 99 |
| 5 | $2.09 \times 10^{-5}$ | $1.458 \times 10^{-5}$ | 0.055 | 0.115 | 196 | 93.6 |

For unconsolidated low-permeability reservoirs, an ideal sand stabilizer should enhance particle stability while maintaining pore throat connectivity. As shown in Figure 6, the treated particles formed more compact aggregates with rough coated surfaces, and localized surface coverage and weak interparticle bonding were observed at high magnification. Visible intergranular voids were still retained, indicating limited stabilization rather than dense pore plugging. This stabilization mode is consistent with previous reports that moderate polymer adsorption can improve sand stability while preserving flow channel connectivity [20] and is beneficial for subsequent self-diverting acid injection.

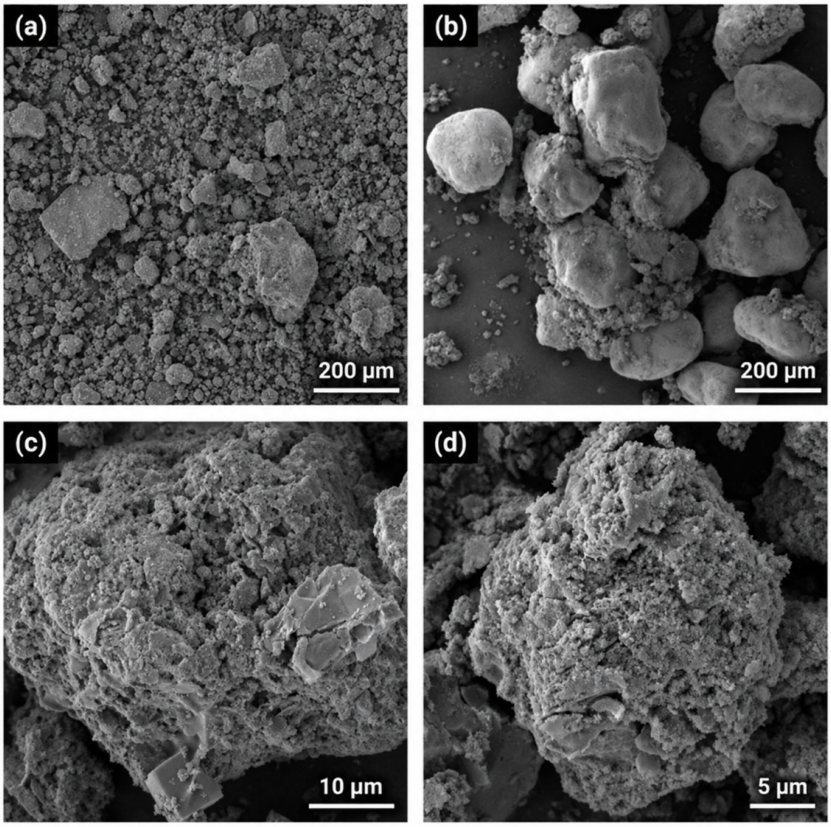



**Figure 6.** SEM images showing the morphology of sand particles and treated particle aggregates at different magnifications: (**a**) low-magnification image of fine sand particles, scale bar = 200 μm; (**b**) low-magnification image of particle aggregates after chemical treatment, scale bar = 200 μm; (**c**) high-magnification image showing local surface coating and particle bonding, scale bar = 10 μm; (**d**) enlarged surface morphology of the treated aggregate, scale bar = 5 μm.

### *3.3. Synergistic Response of the Staged Coupling Process*

#### 3.3.1. Pressure Response of Different Slug Ratios and Control Groups

The pressure response of the integrated treatment was first evaluated by varying the sand-stabilizer-to-main-acid slug ratio. As shown in Figure 7, a 1:1 slug volume ratio generated a pressure of 0.86 MPa during the sand stabilization stage, and subsequent injection of the self-diverting acid increased the pressure to 3.98 MPa. These results indicate that the preplaced stabilizer did not significantly weaken the temporary plugging or diversion capacity of the acid. Under appropriate slug volume and aging conditions, the stabilizer formed limited cementation at grain contacts without causing irreversible plugging of the primary flow channels, allowing the self-diverting acid to penetrate the core and develop flow resistance after the acid–rock reaction.

Four treatment modes were further compared: acidizing alone, sand stabilization alone, sand stabilization followed by acidizing, and the premixing boundary control group. As shown in Figure 8, the staged sand-stabilization-followed-by-acidizing treatment reduced sand production while maintaining a strong pressure response. Relative to acidizing alone, preplaced stabilization mitigated the adverse effects of acid dissolution on framework stability. Relative to sand stabilization alone, the subsequent self-diverting acid improved pore connectivity and enhanced diversion. The premixing boundary control group exhibited strong sand control performance but a more localized increase in pressure, suggesting localized viscosity buildup or front-end interactions when the acid directly contacted the polymer. Accordingly, staged injection is more suitable for field applications than prolonged premixing or simultaneous injection.

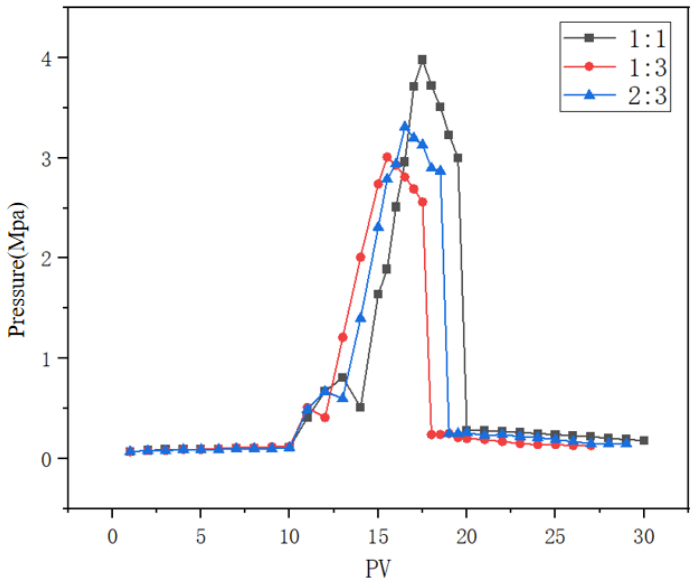



**Figure 7.** Core flooding response at different sand-stabilizer-to-main-acid slug ratios.

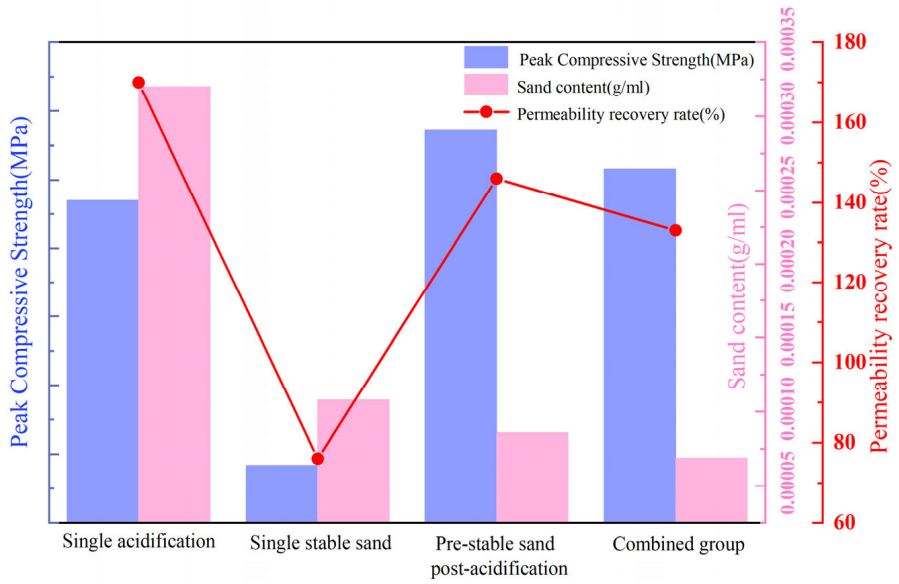



**Figure 8.** Comparison of acidizing alone, sand stabilization alone, staged treatment, and premixing boundary control treatment.

The premixed acid–stabilizer system exhibited a time-dependent viscosity response (Table 10).

**Table 10.** Effects of contact time on the apparent viscosity and visual stability of the premixed acid–stabilizer system.

| Stabilizer-to-Main-Acid Ratio | Contact Time/min | Apparent Viscosity/mPa·s | pH |
|---|---|---|---|
| 1:1 | 0 | 18.6 | 0.72 |
| 1:1 | 5 | 22.4 | 0.76 |
| 1:1 | 10 | 29.8 | 0.81 |
| 1:1 | 30 | 43.7 | 0.93 |
| 1:1 | 60 | 58.9 | 1.08 |
| 1:1 | 120 | 67.5 | 1.21 |
| 1:1 | 240 | 62.8 | 1.34 |

After the optimized 0.2 wt% cationic polyacrylamide stabilizer was directly mixed with the 8 wt% HCl + 3 wt% polyhydrogen acid + 5 wt% EAB self-diverting acid at a 1:1 volume ratio, no obvious precipitation or phase separation was observed within the tested contact period, indicating acceptable static compatibility. However, the apparent viscosity increased from 18.6 mPa·s at 0 min to 58.9 mPa·s at 60 min and reached 67.5 mPa·s at 120 min, followed by a slight decrease to 62.8 mPa·s at 240 min. This result indicates that prolonged direct contact between the acid and the stabilizer may alter the internal fluid structure and promote premature viscosity buildup before the fluid reaches the target pore space.

The dynamic pressure–PV response of the premixing boundary control group was further compared with the 300 mD, 1:1 staged integrated flooding curve (Figure 9).

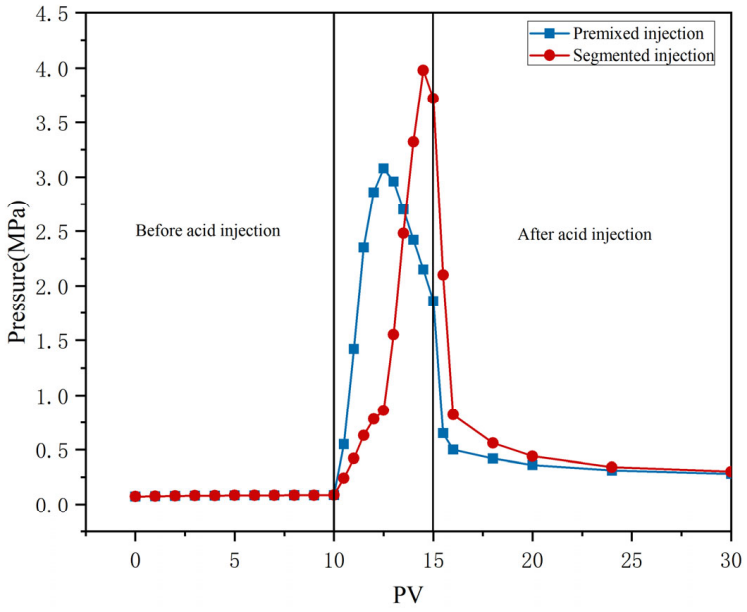



**Figure 9.** Comparison of pressure–PV curves between the 300 mD, 1:1 staged integrated treatment and the premixing boundary control group.

During the formation water baseline stage, the pressure remained stable at 0.072–0.086 MPa, indicating a stable initial flow state. After the premixed acid–stabilizer working fluid entered the core, the pressure increased rapidly from 0.55 MPa at 10.5 PV to 3.08 MPa at 12.5 PV, and then gradually decreased during continued injection. In contrast, the staged integrated treatment showed a more delayed pressure increase: the stabilizer stage produced moderate resistance, and the subsequent self-diverting acid stage reached a peak pressure of 3.98 MPa at approximately 14.5 PV. This comparison indicates that direct premixing shifted the pressure buildup toward an earlier injected-PV interval and promoted a more front-loaded flow resistance response.

The pressure decline during the post-flush stage indicates that part of the premixing-induced flow resistance could be removed by subsequent water flooding; however, the pressure at the end of post-flush injection remained higher than the initial baseline. Together with the contact-time viscosity results, this pressure response suggests that prolonged direct contact between the strong acid and the cationic polymer may induce premature viscosity buildup or localized inlet-side interaction before the acid fully reaches the target pore space. Therefore, the premixing group should be regarded as a boundary control condition for evaluating acid–stabilizer compatibility risk rather than as a recommended field procedure. Compared with premixing, the staged sequence preserves the initial injectivity and placement capacity of the acid while allowing reaction-induced viscosity building and diversion to develop after acid–rock interaction.

3.3.2. Integrated Physical Model Tests at Different Permeabilities

The integrated treatment was evaluated using cores with different absolute permeabilities while considering both particle stability and flow retention [21]. As shown in Figure 10, the system exhibited a strong dependence on permeability. In low-permeability cores, sand stabilization improved particle stability, but the additional flow resistance became more pronounced, limiting permeability retention. In medium-permeability cores, the pore throat space was sufficient to accommodate limited stabilization, and the self-diverting acid continued to access dominant flow channels and develop reaction-induced viscosity. Consequently, acid dissolution and sand stabilization acted synergistically. In high-permeability cores, preferential flow through dominant channels reduced the effectiveness of diversion, resulting in weaker process synergy. These results confirm that the integrated treatment does not represent a simple superposition of acidizing and sand stabilization; instead, its effectiveness depends on rock properties, slug sequence, and material compatibility.

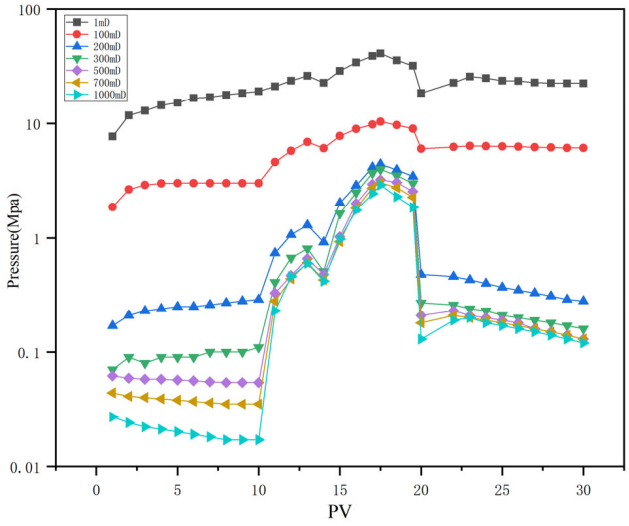



**Figure 10.** Pressure response of the integrated treatment for cores with different permeabilities.

To further evaluate the applicability of the staged integrated treatment under representative reservoir temperature conditions, additional core flooding experiments were conducted at 50 °C using 300 and 500 mD cores. The pressure responses are shown in Figure 11.

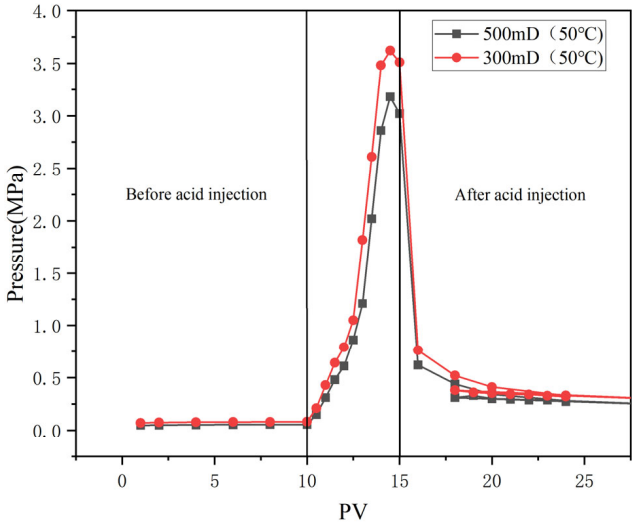



**Figure 11.** Pressure–PV curves of the staged integrated core flooding tests at 50 °C using 300 and 500 mD cores.

During the formation water baseline stage, both cores showed stable low pressure, indicating stable initial flow conditions. After the stabilizer slug was injected, the pressure increased moderately, reflecting limited near-wellbore sand stabilization rather than severe pore throat plugging. When the self-diverting acid was subsequently injected, the pressure increased significantly. Compared with the room-temperature staged treatment, the pressure peaks at 50 °C were slightly lower, indicating partial weakening of the wormlike-micelle entanglement network at an elevated temperature. Nevertheless, the pressure response remained obvious, confirming that the acid system retained effective reaction-induced diversion capacity at reservoir temperature.

### *3.4. Pore Structure Evolution After Staged Treatment*

SEM analysis was conducted on untreated and staged-treatment cores with an approximate permeability of 300 mD, scale bar = 50 μm. The samples consisted of parallel cores from the same batch used for the LF-NMR measurements. Figure 12 shows that the staged-treated core exhibited dissolution features and more distinct pore boundaries, whereas the overall framework remained intact, and no large-scale collapse was observed. Compared with acidizing alone, which induced local fines detachment and particle-edge breakage, the staged-treated sample showed improved pore boundaries while maintaining relatively stable grain morphology. These observations indicate that the stabilizer maintained near-wellbore skeletal stability, whereas the self-diverting acid primarily promoted diversion and damage removal farther from the inlet.

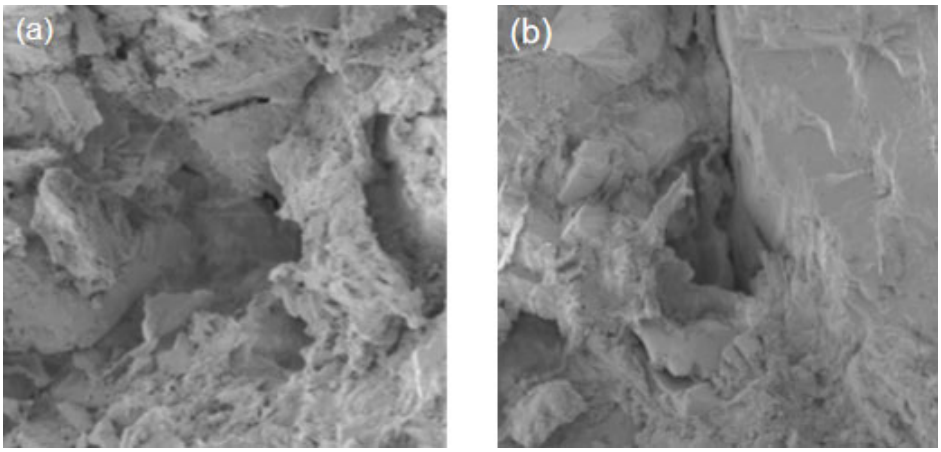



**Figure 12.** SEM micrographs of (**a**) the original core and (**b**) the core after staged acidizing–sand-stabilization treatment.

LF-NMR was used to analyze porosity, pore size distribution, pore throat distribution, and signal intensity before and after staged treatment using parallel 300 mD cores. The samples were saturated with formation water before testing. Figures 13–15 show that staged acidizing–sand stabilization improved pore structure. The signal intensity in the low-permeability region increased after treatment, and the proportion of small and medium pores increased, indicating that the acid penetrated low-permeability regions without disrupting the stabilized framework while promoting the formation of secondary pores.

Total core porosity increased from 7.81% to 9.34%, corresponding to an increase of approximately 19.6%. The principal contribution interval shifted from 6.3–16 μm before treatment to 2.5–10 μm after treatment. The proportions of 2.5–4 and 4–6.3 μm pore throats increased, whereas the proportion of pore throats larger than 10 μm decreased significantly, and the 16–25 μm interval nearly disappeared. These results indicate that the staged treatment increased effective pore space without causing uncontrolled pore-throat coarsening. Instead, the pore structure became more uniform, with pore throats concen-

trated within the medium-size range, reflecting simultaneous pore throat improvement and framework stabilization.

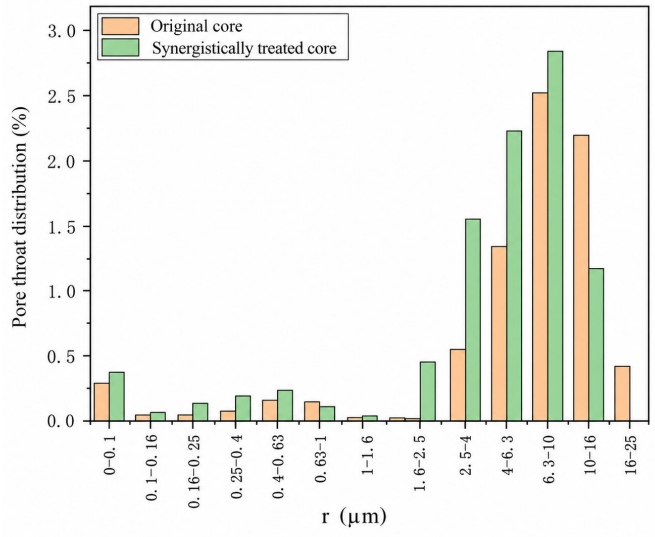



**Figure 13.** Comparison of pore throat distribution before and after staged treatment.

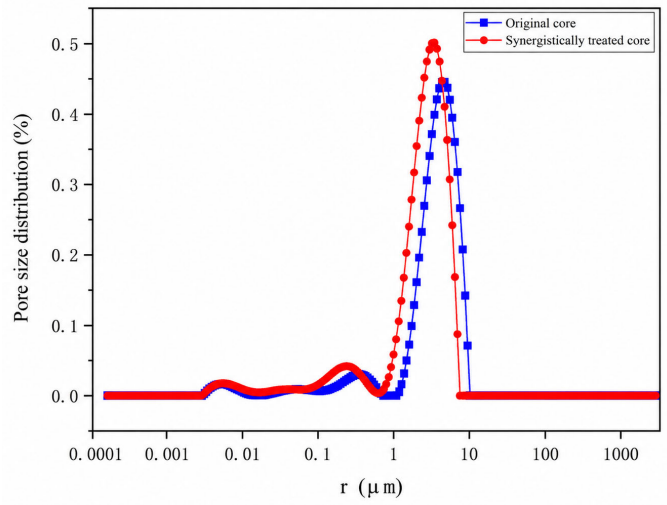



**Figure 14.** Comparison of pore size distribution before and after staged treatment.

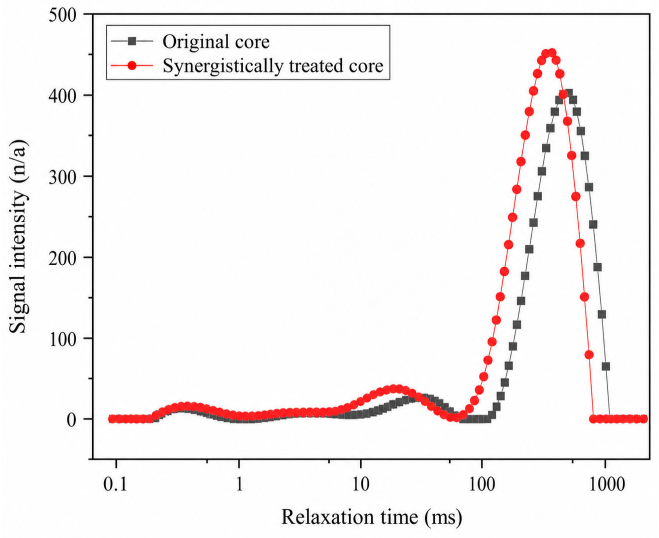



**Figure 15.** Comparison of LF-NMR signal intensity before and after staged treatment.

### *3.5. Synergistic Mechanism and Applicability Window*

The synergy between self-diverting acidizing and sand stabilization resulted from the coordinated matching of treatment timing, spatial placement, and treatment intensity. Direct simultaneous mixing may alter polymer conformation, adsorption, and crosslinking, causing premature viscosity building near the wellbore or in surface lines and reducing deep placement. The stabilizer may also consume reactive acid components or shield the acid–rock reaction interface. Accordingly, the recommended treatment employed a staged sequence rather than simultaneous injection. First, the sand stabilizer slug formed a limited cemented layer in the near-wellbore region, thereby improving particle stability. Second, the self-diverting acid entered the relatively stable high-permeability channels and developed viscosity after the acid–rock reaction. Third, subsequent acid was diverted into lower-permeability zones, allowing deeper stimulation. Figure 16 summarizes this mechanism. The arrows indicate the injection direction, acid flow path, and diversion direction during the staged treatment.

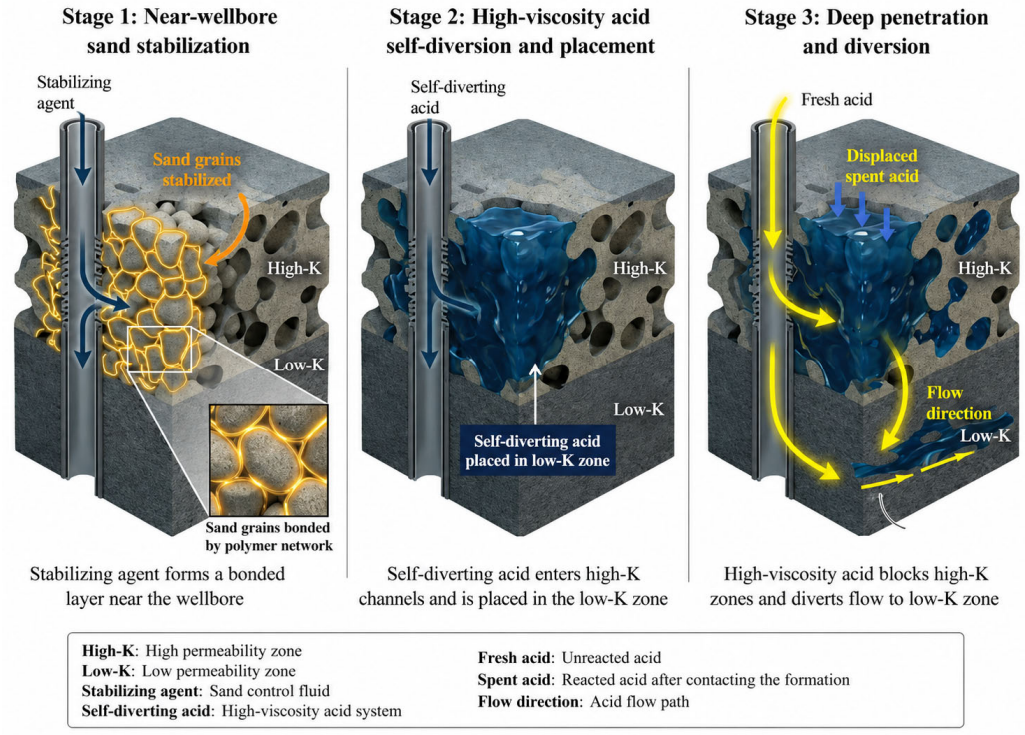



**Figure 16.** Mechanism of staged self-diverting acidizing and chemical sand stabilization.

To quantitatively evaluate the coupled diversion, sand stabilization, and permeability retention performance, a comprehensive evaluation framework was constructed from the three dimensions of resistance increase, sand stabilization, and permeability retention [22]. The resistance-increasing index (*Ir*) was defined as the ratio of the maximum pressure drop during treatment to the baseline pressure drop before treatment:

$$Ir = \Delta P_{max} / \Delta P_0 \quad (2)$$

where $\Delta P_{max}$ is the maximum pressure drop during injection and $\Delta P_0$ is the baseline pressure drop during stable formation water injection before treatment. A higher *Ir* indicates greater buildup of flow resistance and a stronger diversion response.

The sand stabilization index (*Is*) was defined as the ratio of the critical sand production flow rate after treatment to that of the untreated sample:

$$Is = Q / Q_0 \quad (3)$$

where $Q$ is the critical flow rate after sand stabilization treatment and $Q_0$ is the critical sand production flow rate of the untreated sample. A higher $Is$ indicates more effective stabilization of sand particles and the reservoir framework.

The permeability retention index ($Ik$) was defined as the ratio of permeability after treatment to that before treatment:

$$Ik = K/K_0 \tag{4}$$

where $K$ is the permeability after treatment and $K_0$ is the initial permeability before treatment. A higher $Ik$ indicates less additional impairment of reservoir flow capacity during sand stabilization and diversion.

Because these three indices have different dimensions, min–max normalization was applied to enable direct comparison:

$$X' = (X - X_{min})/(X_{max} - X_{min}) \tag{5}$$

where $X$ is the original evaluation indicator, and $X_{min}$ and $X_{max}$ are the minimum and maximum values obtained under the same experimental conditions, respectively. A comprehensive synergy index ($SI$) was then defined as follows:

$$SI = 0.4\ Ir' + 0.3\ Is' + 0.3\ Ik' \tag{6}$$

The diversion effect of the self-diverting acid primarily governed the overall pressure response; therefore, the resistance-increasing index was assigned a weight of 0.4, whereas the sand stabilization and permeability retention indices were each assigned weights of 0.3. A higher $SI$ indicates better coordination among self-diverting acid diversion/permeability enhancement, near-wellbore sand stabilization, and permeability retention. According to the normalized experimental results, $SI < 0.40$ was defined as a low-efficiency zone, $0.40 \leq SI < 0.70$ as a moderate-synergy zone, and $SI \geq 0.70$ as a high-synergy zone (see Tables 11 and 12).

**Table 11.** Evaluation indices of the integrated treatment under different permeability conditions.

| Perm., mD | $\Delta P_0$, MPa | $\Delta P_{max}$, MPa | $Q_0$, mL·min$^{-1}$ | Q, mL·min$^{-1}$ | $K_0$, mD | K, mD |
|---|---|---|---|---|---|---|
| 1 | 12.3400 | 40.9100 | 3.4 | 4.0 | 0.5570 | 0.2507 |
| 100 | 2.6960 | 10.3600 | 2.9 | 3.3 | 2.5496 | 1.4788 |
| 200 | 0.1620 | 4.4200 | 2.60 | 3.0 | 45.1950 | 34.8000 |
| 300 | 0.0840 | 3.9800 | 2.5 | 2.9 | 81.8298 | 70.3737 |
| 500 | 0.0588 | 3.2300 | 2.3 | 2.7 | 116.8998 | 102.8718 |
| 700 | 0.0395 | 3.0600 | 2.05 | 2.21 | 202.0600 | 149.5240 |
| 1000 | 0.0228 | 2.9200 | 2.0 | 2.1 | 301.4783 | 205.0053 |

**Table 12.** Calculated synergy indices of the integrated treatment under different permeability conditions.

| Perm., mD | Ir | Is | Ik | Ir′ | Is′ | Ik′ | SI |
|---|---|---|---|---|---|---|---|
| 1 | 1.1985 | 1.176 | 0.45 | 0.0000 | 1.0000 | 0.0000 | 0.3000 |
| 100 | 1.3462 | 1.138 | 0.58 | 0.0404 | 0.6953 | 0.3023 | 0.3154 |
| 200 | 2.8500 | 1.154 | 0.77 | 0.4520 | 0.8254 | 0.7442 | 0.6517 |
| 300 | 3.8582 | 1.160 | 0.86 | 0.7279 | 0.8698 | 0.9535 | 0.8381 |
| 500 | 4.0061 | 1.174 | 0.88 | 0.7683 | 0.9798 | 1.0000 | 0.9013 |
| 700 | 4.4500 | 1.079 | 0.74 | 0.8898 | 0.2302 | 0.6744 | 0.6273 |
| 1000 | 4.8526 | 1.050 | 0.68 | 1.0000 | 0.0000 | 0.5349 | 0.5605 |

To further characterize the variation in process synergy under different permeability conditions, the comprehensive synergy index was calculated from the pressure response, sand stabilization enhancement, and permeability recovery, and its relationship with permeability is presented in Figure 17. The background colors indicate different synergy levels: green represents low synergy ($SI < 0.4$), pink represents moderate synergy ($0.4 \leq SI < 0.7$), and blue represents high synergy ($SI \geq 0.7$).

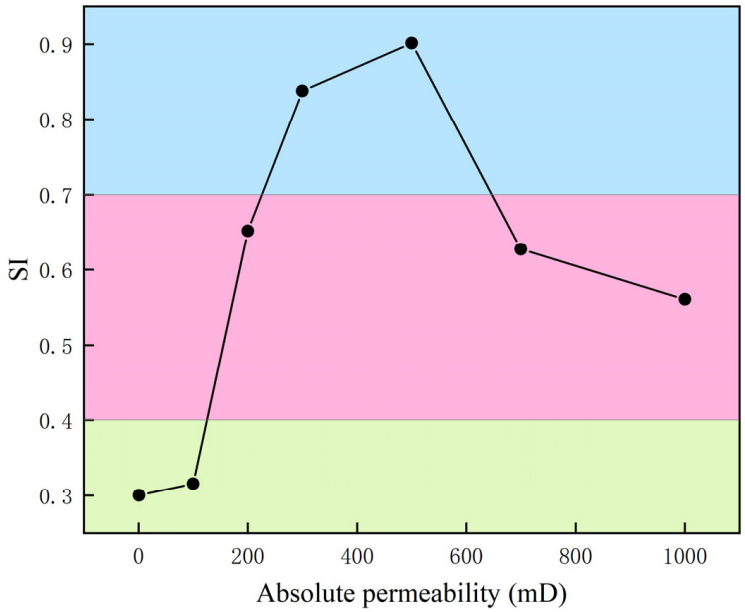



**Figure 17.** Variation in the comprehensive synergy index of the integrated treatment under different permeability conditions.

Figure 17 shows that the comprehensive synergy index exhibited a distinct interval-dependent variation with permeability. The *SI* reached its highest values within the range of 300–500 mD, indicating that the medium-permeability formations provided the most favorable conditions for coordinating temporary plugging by the self-diverting acid, near-wellbore sand stabilization, and post-treatment permeability retention. Under low-permeability conditions, the overall performance was limited by poor permeability recovery. Under high-permeability conditions, overall performance was constrained by insufficient sand stabilization enhancement and pronounced preferential flow through dominant channels. Consequently, both low- and high-permeability samples exhibited weaker overall synergy than medium-permeability samples.

Overall, the performance of the integrated treatment depended on three key matching criteria: (1) whether the residual acid viscosity-building capacity was sufficient to modify flow resistance in dominant channels; (2) whether the sand stabilization strength improved particle stability without introducing excessive formation damage [23]; and (3) whether the permeability contrast was sufficient to promote effective diversion. Accordingly, the applicability of the proposed process is governed by the compatibility among these factors. Under the present experimental conditions, the medium-permeability range offered the most favorable balance for achieving permeability enhancement and sand control.

To examine whether the conclusion depended on the selected *SI* weights, a weight sensitivity analysis was performed, as shown in Table 13.

Under the original weight set of 0.4/0.3/0.3, the *SI* values of the 300 and 500 mD groups were 0.838 and 0.901, respectively. Under equal weights, diversion-prioritized weights, sand-stabilization-prioritized weights, and permeability-retention-prioritized weights, the 300–500 mD range still remained the highest-performing interval. Although the

*SI* values of the 700 and 1000 mD groups increased slightly under the diversion-prioritized scenario, because of their relatively lower baseline pressure and stronger apparent pressure response sensitivity, they still did not exceed the 300–500 mD range. This indicates that the favorable permeability range was not an artifact of a single subjective weight set.

**Table 13.** Weight sensitivity analysis of the comprehensive synergy index.

| Perm./ mD | Original 0.4/0.3/0.3 | Equal 1/3/1/3/1/3 | Diversion-Prioritized 0.5/0.25/0.25 | Sand-Stabilization-Prioritized 0.3/0.4/0.3 | Permeability-Retention-Prioritized 0.3/0.3/0.4 |
|---|---|---|---|---|---|
| 1 | 0.300 | 0.317 | 0.278 | 0.315 | 0.339 |
| 100 | 0.315 | 0.329 | 0.291 | 0.341 | 0.353 |
| 200 | 0.652 | 0.674 | 0.628 | 0.688 | 0.666 |
| 300 | 0.838 | 0.847 | 0.814 | 0.863 | 0.871 |
| 500 | 0.901 | 0.894 | 0.873 | 0.922 | 0.929 |
| 700 | 0.627 | 0.602 | 0.675 | 0.574 | 0.585 |
| 1000 | 0.561 | 0.534 | 0.631 | 0.498 | 0.521 |

The integrated process requires the acid slug to enter the porous medium, build residual acid viscosity at an appropriate position, and divert the subsequent acid without causing excessive permeability impairment. Meanwhile, the cationic polymer must stabilize particles without forming strong inlet plugging. Parallel verification and weight sensitivity analysis confirmed that, under the present experimental conditions, the 300–500 mD range provided the most favorable balance among these processes. Therefore, this interval is described as a favorable permeability range under the present experimental conditions rather than an absolute optimal window.

## 4. Conclusions

1. Low-pressure unconsolidated sandstone gas reservoirs exhibit coupled issues of plugging, heterogeneity, and sand production. Acidizing alone and sand stabilization alone cannot simultaneously provide permeability enhancement and stable production. The proposed integrated treatment consists of a staged synergistic process centered on limited near-wellbore sand stabilization followed by deep self-diverting acid stimulation, rather than a simple premixed acid–stabilizer system.
2. The 5 wt% EAB self-diverting acid system exhibited strong reaction-induced viscosity-building capacity, and the 8 wt% HCl + HF system produced a strong temporary-plugging and diversion response. SEM–EDS results indicate that acidizing improved pore connectivity but also caused localized cement dissolution and fines detachment. These findings demonstrate that effective permeability enhancement must be accompanied by framework stabilization. Temperature-dependent residual acid viscosity tests further showed that the 5 wt% EAB system maintained effective viscosity building at representative reservoir temperature, with a viscosity of 118.7 mPa·s at 50 °C under 8 wt% $CaCO_3$, although higher temperature and excessive $Ca^{2+}$ weakened the micellar network.
3. The optimized 0.2 wt% cationic polyacrylamide (80-mesh) significantly increased the critical sand-production flow rate while maintaining low sand production under high flushing rates. The stabilization mechanism involved adsorption, polymer-chain bridging, and limited cementation at particle contacts rather than extensive pore throat plugging.
4. Staged sand stabilization followed by self-diverting acidizing reduced the risk of sand production while maintaining the pressure response and diversion capability of the acid. The premixing boundary control results suggest that prolonged direct contact between the strong acid and the stabilizer may cause premature localized viscosity building or reaction front displacement, thereby reducing deep placement.

5. The integrated treatment was governed by the residual acid viscosity-building capacity, sand stabilization strength, slug sequence, and permeability contrast. The 300–500 mD medium-permeability range exhibited the best synergy among permeability enhancement, sand control, and permeability retention. Low-permeability formations required damage control, whereas high-permeability formations required enhanced diversion or multistage slug designs.

**Author Contributions:** Conceptualization, Y.P. and S.C.; Methodology, Y.P. and S.C.; Formal analysis, Y.P.; Investigation, Y.P., S.Z., L.L., Q.J. and D.G.; Data curation, Y.P.; Writing—original draft, Y.P.; Writing—review and editing, Y.P. and S.C.; Supervision, S.C.; Project administration, S.C. All authors have read and agreed to the published version of the manuscript.

**Funding:** This research received no external funding.

**Data Availability Statement:** The data presented in this study are available from the corresponding author upon reasonable request.

**Acknowledgments:** The authors acknowledge Xi'an Petroleum University and PetroChina Qinghai Oilfield Company for providing laboratory support and core/material samples used in this study.

**Conflicts of Interest:** Authors Li Liao and Qi Jiang were employed by the Oil and Gas Technology Institute, PetroChina Qinghai Oilfield Company. Author Dan Gao was employed by the Sixth Oil Production Plant of Changqing Oilfield Branch. The remaining authors declare that the research was conducted in the absence of any commercial or financial relationships that could be construed as a potential conflict of interest.

## Abbreviations

| | |
|---|---|
| EAB | Erucamidopropyl Betaine |
| OAB | Oleamidopropyl Betaine |
| APDEMS | Aminopropyl Diethoxy Methylsilane |
| CPAM | Cationic Polyacrylamide |
| EDS | Energy-Dispersive Spectroscopy |
| HF | Hydrofluoric Acid |
| HMDSO | Hexamethyldisiloxane |
| LF-NMR | Low-Field Nuclear Magnetic Resonance |
| PAM | Polyacrylamide |
| PV | Pore Volume |
| SEM | Scanning Electron Microscopy |
| VES | Viscoelastic Surfactant |

## References

1. Tang, H.; Meng, Y.; He, S.; Li, G.; Zhang, W. Sand production and sand-control mechanisms in unconsolidated sandstone gas reservoirs in the eastern Qaidam Basin. *Nat. Gas Ind.* **2002**, *22*, 52–54. (In Chinese)
2. Zhao, B.; Su, Y.; Cong, W.; Sun, H.; Dong, X.; Hu, M.; Li, Y. Discrete-element analysis of sand-production risk and mechanism in sandstone oil and gas reservoirs. *J. Saf. Sci. Technol.* **2020**, *16*, 59–65. (In Chinese)
3. Cui, S.H.; Zhu, H.Y.; Zhong, S. Reservoir properties variation characteristics and stress sensitivity of Sebei Gas Field and its influence on gas field development. *Nat. Gas Geosci.* **2008**, *19*, 141–144. (In Chinese)
4. Wang, F.; Zhang, Z.; Liao, L.; Chen, J.; Zhang, W.; Feng, D.; Zhao, Y.; Jiang, Q. Mechanism of mud and sand plugging in unconsolidated sandstone gas reservoirs. *Pet. Geol. Recovery Effic.* **2023**, *30*, 137–146. (In Chinese)
5. Li, C.; Chen, X.; Li, P.; Zhang, C.; Ma, P. Preparation and Property of Membrane Stabilizer System for Weakly Consolidated Sandstone Reservoir. *Oilfield Chem.* **2020**, *37*, 58–61. (In Chinese)
6. Al-Shargabi, M.; Davoodi, S.; Wood, D.A.; Ali, M.; Rukavishnikov, V.S.; Minaev, K.M. A critical review of self-diverting acid treatments applied to carbonate oil and gas reservoirs. *Pet. Sci.* **2023**, *20*, 922–950. [CrossRef]
7. Zheng, N.; Zhu, J.; Yang, Z.; Li, X.; Chen, H.; Su, H.; Qiao, L. Molecular dynamics simulation and key performance study of VES self-diverting acid system for deep carbonate reservoirs. *J. Mol. Liq.* **2024**, *401*, 124645. [CrossRef]

8. Safaei, A.; Asefi, M.; Ahmadi, M.; Pourshamsi, T.; Baloochestanzadeh, S.; Khalilnezhad, A.; Riazi, M. Chemical treatment for sand production control: A review of materials, methods, and field operations. *Pet. Sci.* **2023**, *20*, 1640–1658. [CrossRef]
9. Xu, Z.; Shen, K.; Zhou, J.; Huang, Q.; Liu, P.; Du, J.; Wu, J. Chemical sand production control: A review of materials, methods, and characterization. *Front. Energy Res.* **2024**, *12*, 1424059. [CrossRef]
10. Ali, M.; Viktorivich, K.V.; Vitalievich, S.P.; Igorovna, B.K.; Mohammed, A.-S. Development of viscoelastic surfactant-based self-diverting acid system to stimulate oil production in carbonate reservoirs. In *Proceedings of the International Field Exploration and Development Conference*; Springer: Singapore, 2023; pp. 3415–3424. [CrossRef]
11. Jiang, G.; Guo, X.; Li, D. Design and application of deep sand firming formula in unconsolidated sandstone. *Chin. J. Appl. Chem.* **2007**, *24*, 796–800. (In Chinese)
12. Lei, X. Sand Production Mechanism and Control Method for Fractured Tight Sandstone Gas Wells. Ph.D. Thesis, Southwest Petroleum University, Chengdu, China, 2023. (In Chinese)
13. Li, Q.; Wang, F.; Wu, J.; Li, Q.; Zhang, G. Multivariate Coupling Model and Reservoir Characteristics of Enhanced Geothermal Reservoirs. *Energies* **2026**, *19*, 3180. [CrossRef]
14. Li, Q.; You, D.; Li, Q.; Wang, F.; Wang, Y.; Yang, Y. Analysis of Sedimentation Behavior and Influencing Factors of Solid Particles in $CO_2$ Fracturing Fluid. *Processes* **2025**, *13*, 4049. [CrossRef]
15. Li, Q.; Li, Q.; Wu, J.; He, K.; Xia, Y.; Liu, J.; Wang, F.; Cheng, Y. Wellhead Stability During Development Process of Hydrate Reservoir in the Northern South China Sea: Sensitivity Analysis. *Processes* **2025**, *13*, 1630. [CrossRef]
16. Marandi, S.Z.; Salehi, M.B.; Moghadam, A.M. Sand control: Experimental performance of polyacrylamide hydrogels. *J. Pet. Sci. Eng.* **2018**, *170*, 430–439. [CrossRef]
17. Salehi, M.B.; Moghadam, A.M.; Marandi, S.Z. Polyacrylamide hydrogel application in sand control with compressive strength testing. *Pet. Sci.* **2019**, *16*, 94–104. [CrossRef]
18. Guo, J.C.; Zhou, H.Y.; Zeng, J.; Wang, K.J.; Liu, Y.X. Advances in low-field nuclear magnetic resonance technologies applied for characterization of pore space inside rocks: A critical review. *Pet. Sci.* **2020**, *17*, 1281–1297. [CrossRef]
19. ManzariTavakkoli, M.H.; Sedaee, B.; Mahmoodi, A. Numerical investigation of acid diversion using viscoelastic surfactant (VES) under single and two-phase flow conditions. *J. Pet. Explor. Prod. Technol.* **2025**, *15*, 37. [CrossRef]
20. Wei, Z.; Zhu, L.; Zhang, Y.; Meng, K.; Zuo, Q.; Hu, x. Laboratory performance evaluation of chemical sand stabilizers for unconsolidated sandstone reservoirs. *Fine Petrochem. Ind.* **2025**, *42*, 1–4. (In Chinese)
21. Zhang, D. Accumulation conditions and key technologies for exploration and development in Sebei Gas Field in Qaidam Basin, NW China. *Pet. Res.* **2019**, *4*, 191–210. [CrossRef]
22. Yang, X. Study on Diversion Boundary of Acidizing in Carbonate Reservoirs. Master's Thesis, China University of Petroleum (East China), Qingdao, China, 2022. (In Chinese)
23. Gussenov, I. Literary review: Permeability alterations in sandstone after acidizing. *Energy Rep.* **2023**, *9*, 6328–6348. [CrossRef]


**Disclaimer/Publisher's Note:** The statements, opinions and data contained in all publications are solely those of the individual author(s) and contributor(s) and not of MDPI and/or the editor(s). MDPI and/or the editor(s) disclaim responsibility for any injury to people or property resulting from any ideas, methods, instructions or products referred to in the content.